Postsynaptic gephyrin clustering controls the development of adult-born granule cells in the olfactory bulb

Postsynaptic gephyrin clustering controls the development of adult-born granule cells in the olfactory bulb

Francine Deprez[1,2], Marta Pallotto[3], Fabia Vogt[1], Marta Grabiec[1,4], Mari A. Virtanen[5], Shiva K. Tyagarajan[1,2], Patrizia Panzanelli[6], Jean-Marc Fritschy[1,2]

[1]University of Zurich, Institute of Pharmacology and Toxicology, 8057 Zurich, Switzerland

[2]Neuroscience Center Zurich, ETH and University of Zurich

[3]Circuit Dynamics and Connectivity Unit, National Institute of Neurological Disorders and Stroke, National Institute of Health Bethesda, MD, USA

[4]Present address: Masaryk University, Dept. of Biology, 625 00 Brno, Czech Republic

[5]Dept. Neurosciences fondamentales CMU, University of Geneva, 1211 Geneva, Switzerland

[6]University of Turin, Dept. of Neuroscience Rita Levi Montalcini, Turin, Italy

Running Head: Gephyrin regulation of neuronal development

Proposed Associate Editor: Dr. John L. R. Rubenstein

Key Words: Adult neurogenesis; dendrites; GABA; lentiviruses; postsynaptic density; phosphorylation; spines; RRID:AB_1586992, RRID:AB_10000240, RRID:AB_887725, RRID:AB_887717, RRID:AB_1501344, RRID:AB_887869, RRID:AB_887869, RRID:AB_2315546

Correspondence : Dr. Jean-Marc Fritschy, University of Zurich, Institute of Pharmacology and Toxicology, Winterthurerstrasse 190, 8057 Zurich, Switzerland; e-mail: fritschy@pharma.uzh.ch

Grant support: This study was supported by the Swiss National Science Foundation (Grant 310030_146120 to JMF and international short-visit grant to MP) and by an IBRO-SNSF grant of the Swiss Society for Neuroscience (PAIBP3–133278 to MG).

Abstract

In adult rodent olfactory bulb, GABAergic signaling regulates migration, differentiation, and synaptic integration of newborn granule cells (GCs), migrating from the subventricular zone. Here, we show that these effects depend on the formation of a postsynaptic scaffold organized by gephyrin - the main scaffolding protein of GABAergic synapses, which anchors receptors and signaling molecules to the postsynaptic density - and are regulated by the phosphorylation status of gephyrin. Using lentiviral vectors to selectively transfect adult-born GCs, we observed that overexpression of the phospho-deficient gephyrin mutant eGFP-gephyrin(S270A), which facilitates the formation of supernumerary GABAergic synapses *in vitro*, favors dendritic branching and formation of transient GABAergic synapses on spines, identified by the presence of α2-$GABA_A$Rs. In contrast, overexpression of the dominant-negative eGFP-gephyrin(L2B) (a chimera that is enzymatically active but clustering defective), curtailed dendritic growth, spine formation, and long-term survival of GCs, pointing to the essential role of gephyrin cluster formation for its function. We could exclude any gephyrin overexpression artefacts, as GCs infected with eGFP-gephyrin were comparable to those infected with eGFP alone. The opposite effects induced by the two gephyrin mutant constructs indicate that the gephyrin scaffold at GABAergic synapses orchestrates signaling cascades acting on the cytoskeleton to regulate neuronal growth and synapse formation. Specifically, gephyrin phosphorylation emerges as a novel mechanism regulating morphological differentiation and long-term survival of adult-born olfactory bulb neurons.

Introduction

Adult neurogenesis is an important facet of brain plasticity and provides a powerful model for investigating mechanisms of neuronal differentiation and functional integration into existing circuits in the adult brain (Lepousez et al., 2013; Ming and Song, 2011; Pallotto and Deprez, 2014; Whitman and Greer, 2009). Olfactory bulb (OB) granule cells (GCs) are constantly replaced during adult life from a pool of progenitor cells in the subventricular zone. These axonless interneurons control lateral inhibition and synchronization of principal cells (Lagier et al., 2007; Lledo et al., 2006). Their differentiation and synaptic integration is regulated by GABAergic signaling (reviewed in (Bovetti et al., 2011; Gascon et al., 2006; Ge et al., 2006; Ge et al., 2007; Nissant and Pallotto, 2011; Platel et al., 2007)), but the underlying mechanisms are unclear. The present study was designed to test whether signaling cascades associated with the GABAergic postsynaptic density regulate growth and differentiation of adult-born neurons.

This hypothesis is based on the previous observation that targeted deletion of *Gabra2* in adult-born GCs, strongly reduces GABAergic signaling and curtails their morphological differentiation, as well as formation of afferent and dendro-dendritic synapses (Pallotto et al., 2012). Further, *Gabra2*-deficient GCs are unable to adapt morphologically to sensory enrichment or deprivation, suggesting a key role for α2-$GABA_A$Rs in modulating neuronal development and plasticity (Pallotto et al., 2012). However, the targeted deletion of *Gabra2* in newborn GCs also disrupts postsynaptic clustering of gephyrin, the major scaffolding protein of GABAergic and glycinergic synapses. Gephyrin interacts with various signaling molecules, notably protein kinases and phosphatases, the protease calpain, the RhoGEF collybistin, and modulators of the actin cytoskeleton (Tyagarajan and Fritschy, 2014). In addition, gephyrin is subject to extensive post-translational modifications, which regulate its scaffolding and postsynaptic clustering properties. In particular, gephyrin phosphorylation at serine 270 (S270) modulates both GABAergic synaptic function and dendrite development *in vitro* (Kuhse et al., 2012; Rui et al., 2013; Tyagarajan et al., 2011). Further, interaction of gephyrin with signaling molecules that regulate the cytoskeleton influences spine formation and plasticity (Tyagarajan and Fritschy, 2014). Therefore, we reasoned that gephyrin scaffold disruption in *Gabra2*-null neurons might affect downstream signaling and impair their differentiation and maturation.

To test this hypothesis and investigate the role of gephyrin in regulating neuronal differentiation and plasticity, we generated lentiviruses (LV) to deliver eGFP-tagged rat P2 gephyrin (Geph), or Geph(S270A), with a point-mutation abolishing S270 phosphorylation and facilitating GABAergic synapse formation in cultured hippocampal neurons (Tyagarajan et al., 2011), or Geph(L2B), a chimeric gephyrin engineered with a 6-residue substitution in a

surface-exposed loop (L2B) of the gephyrin E-domain that abolishes gephyrin postsynaptic clustering (Lardi-Studler et al., 2007). LVs were injected stereotaxically into the rostral migratory stream of adult mice to infect neural precursors migrating towards the OB (Panzanelli et al., 2009). Using immunofluorescence and immuno-electron microscopy, we investigated the impact of gephyrin overexpression and postsynaptic clustering on maturation and synapse structure of adult-born GCs, and on their long-term survival. We focused on dendrite development, spine growth, and GABAergic synapse formation.

Our data indicate that adequate gephyrin clustering is necessary for proper neuronal development and survival, emphasizing the crucial role played by the gephyrin scaffold for organizing signaling cascades downstream of GABAergic synapses.

Materials and Methods

Animals

All experiments were performed using 8-12 week-old male C57BL/6/JOlaHsd mice (Harlan Laboratories, The Netherlands), which were bred in the animal facility of the Institute of Pharmacology and Toxicology at the University of Zurich.

Lentiviral vectors

LVs encoding the eGFP constructs were produced by transfecting HEK 293T cells with four separate plasmids containing the transgene under the control of the phosphoglycerate kinase (PGK) promoter (eGFP, eGFP-Geph, eGFP-Geph(S270A) and eGFP-Geph(L2B)), packaging and coat. The supernatant containing the virus was concentrated by ultracentrifugation and diluted in PBS. Typically, the preparations used had a titer of 10^8 cfu/mL, as determined upon HEK293 cell transfection. The LV encoding tdTomato (UbC-TdTomato-WPRE; origin plasmid: FUtdTW (Addgene Plasmid #22478) was generously provided by the laboratory of Dr. P.M. Lledo (Institut Pasteur, Paris). Its titer, determined by qPCR, was $8*10^9$ VG/mL.

Stereotaxic injections

Adult male mice were anesthetized by inhalation with 2.5-3% isoflurane (Baxter) in oxygen and placed on the stereotaxic frame (David Kopf Instruments). The mice received a bilateral injection of viral particles (200 nL) into the RMS (antero-posterior (AP) = +3.3 mm, medio-lateral (ML) = ±0.82 mm, dorso-ventral (DV) = -2.9 mm, with Bregma as reference), using a nanoliter injector Nanoject II (Drummond Scientific). After the surgery, the mice received an i.p. injection of 1 mg/kg buprenorphine (Temgesic, Essex Chemicals, Lucerne, Switzerland) and were placed on a warm pad for recovery before being returned to their home cage.

Tissue preparation for immunohistochemistry

Mice were deeply anesthetized with pentobarbital (Nembutal®; 50 mg/kg, i.p.) and perfused transcardially with 15-20 mL ice-cold, oxygenated artificial cerebrospinal fluid (ACSF), pH 7.4, as described (Notter et al., 2014). After perfusion, the mice were decapitated immediately on ice and the OB was dissected out and fixed by immersion in 4% paraformaldehyde (dissolved in 0.15 M sodium phosphate buffer, pH 7.4) for 90 min. After cryoprotection overnight in 30% sucrose, 50-μm-thick horizontal or coronal sections from frozen OB were cut with a sliding microtome and collected in phosphate-buffered saline (PBS).

Immunofluorescence staining

Double and triple immunofluorescence staining was performed by incubating OB sections with the primary antibody (Table 1) diluted in PBS (pH 7.4) containing 2% normal donkey serum and 0.2% Triton X-100 for 48-72 h at 4°C.

Sections were then washed in 3x PBS for 10 min and incubated at room temperature in secondary antibodies raised in donkey and conjugated to Alexa 488 (Invitrogen), Cy3, or Cy5 (Jackson ImmunoResearch). Afterwards, sections were rinsed again 3 times in PBS, mounted on gelatin-coated slides, air-dried, and coverslipped with fluorescence mounting medium (Dako).

Characterization of antibodies

The GST-depleted guinea pig antibody against doublecortin (DCX; RRID:AB_1586992) was raised using a C-terminal peptide. Its specificity was determined by Western blot analysis and immunohistochemistry of rodent brain lysates, recognizing selectively adult-born neurons in the dentate gyrus, rostral migratory stream, and olfactory bulb (Ledergerber et al., 2006).

The chicken IgY fraction from yolks against GFP (RRID:AB_10000240) was raised using purified recombinant GFP. Its specificity was determined by Western blot analysis and immunohistochemistry using transgenic mice expressing the GFP gene product

The rabbit polyclonal antiserum against GFP (RRID:AB_887725) was raised using Strep-Tag full-length fusion protein. It cross-reacts with GFP-derivatives and was characterized by immunohistochemistry using transgenic mice expressing the GFP gene product (Zeilhofer et al., 2005).

The affinity purified guinea pig polyclonal antibody against the $GABA_AR$ $\alpha 2$ subunit was raised using a rat N-terminal synthetic peptide 1–9 (NIQEDEAKN-C) coupled to keyhole lymphet hemocyanin (KLH). It was characterized extensively by biochemistry (Western blotting, immunoprecipitation) and by immunohistochemistry using tissue from *Gabra2*-knockout mice (Panzanelli et al., 2011).

The mouse monoclonal mAb7a against gephyrin (RRID:AB_887717) was raised using affinity-purified rat glycine receptors. It is widely used to detect gephyrin in inhibitory synapses, as well as recombinant gephyrin expressed in neurons (Lardi-Studler et al., 2007; Sassoè-Pognetto et al., 2000).

The affinity-purified rabbit polyclonal antibody against vGAT (RRID:AB_887869) was raised using a rat synthetic peptide 75-87 (AEPPVEGDIHYQR). Its specificity for the mammalian vGAT was demonstrated by Western blotting and immunohistochemistry (selective detection of GABAergic terminals in CNS sections and primary neuron cultures) (Brünig et al., 2002; Dumoulin et al., 1999).

The guinea pig polyclonal antiserum against vGAT (RRID:AB_887869) was raised using a Strep-Tag fusion protein of rat VGAT (aa. 2-115). Its specificity was determined by comparison with the staining pattern obtained with the rabbit polyclonal antibody.
The rabbit polyclonal serum against vGluT1 (RRID:AB_2315546) was raised using a recombinant GST-fusion protein containing amino acid residues 456-561 of rat vGluT1. Its specificity for the mammalian vGluT1 demonstrated by Western blotting and immunohistochemistry (Bellocchio et al., 2000; Fujiyama et al., 2001; Todd et al., 2003)

Lucifer Yellow experiment

Five mice injected with eGFP-Geph were deeply anesthetized with Nembutal® at 21 days post-injection (dpi) and perfused transcardially with ice-cold 0.9% NaCl followed by ice-cold 4% paraformaldehyde, 0.125% glutaraldehyde solution (pH 7.4). After postfixation for 2 h in 4% paraformaldehyde, 300-μm-thick horizontal OB sections were cut with a vibrating microtome and placed in an injection chamber in an Olympus microscope equipped with a micromanipulator. Single eGFP-Geph-positive GCs visualized by epifluorescence were filled iontophoretically with a 0.4% Lucifer Yellow solution (Sigma-Aldrich, St. Louis, MO), using a sharp micropipette. A negative current of 70 nA was applied until the dendrites were fluorescing brightly.
To detect Lucifer Yellow, OB sections were incubated with rabbit antibodies to Lucifer Yellow (RRID:AB_1501344) diluted 1:4000 in PBS containing sucrose (5%), bovine serum albumin (2%), Triton X-100 (1%), and Na azide (0.1%), for 48 h at room temperature. Sections were then washed in PBS and incubated for another 48 h with a secondary antibody conjugated to Alexa 488 (Invitrogen; 1:1000). Afterwards, sections were washed in PBS, mounted and coverslipped with fluorescence mounting medium (Dako).

Image acquisition and analysis

Sections from all LV-injected mice were examined by epifluorescence microscopy after staining for GFP. Samples that contained either no eGFP-positive cells or cells distributed only in a small sector of the OB were discarded from further analysis. Data collection was done by laser-scanning microscopy (LSM700, Carl Zeiss GmbH, Germany), using sequential acquisition of separate wavelength channels to avoid fluorescence crosstalk.
To determine their survival rate, tdTomato-, eGFP-Geph(S270A)- and eGFP-Geph(L2B)-positive GCs were counted from 5-7 randomly selected coronal sections per mouse (anterior to the accessory olfactory bulb; 4-5 mice/group) and averaged per section. Dual acquisition mode was used to determine the fraction of double-labeled cells. The radial migration distance from the RMS was determined for a subset of 18-23 green and red cells/section,

both as the absolute distance covered by the cell and as the relative fraction of the GCL thickness.

To investigate the total length and number of branches of the dendritic tree of adult-born GCs, GFP-positive GCs were selected randomly in the GCL (n=17-20 cells per mouse; 3-6 mice/group) from 50-um-thick sections. The entire cell was acquired, taking z-stacks spaced by 0.5 um. Dendritic morphometry was analyzed with the NeuronJ plug-in from the software NIH ImageJ.

Sholl analysis was performed with concentric circles, spaced at 10 μm intervals, centered on the cell body. The numbers of intersections were calculated using a Sholl Analysis plugin (Anirvan Ghosh Laboratory, University of California, San Diego, La Jolla, CA). For statistical comparison, the area under the curve (AUC) of the resulting function was calculated. Quantifications were performed on 13-20 cells from 3-6 mice of each experimental group.

The average number of spines, per unit length, on GFP-positive GCs (n=10-20 segments per mouse; 3-6 mice per construct) was calculated on 3D-projected image stacks with ImageJ software.

Localization of α2-subunit-positive clusters in spines or dendritic shafts of LV-infected GCs was determined manually in 3D images, using the co-localization module of the Imaris software (Bitplane, Switzerland; version 7.4). Quantification was done per unit length (measured on the same image). Total number of clusters was calculated based on average total dendritic length calculated in the morphometric analysis.

Pre-embedding electron microscopy

Stereotaxic injections of LVs were performed as described above in 6 mice per gephyrin construct assayed (eGFP-Geph, eGFP-Geph(S270A), eGFP-Geph(L2B)). At 21 dpi, they were deeply anesthetized with Nembutal and perfused with ice-cold 2% paraformaldehyde and 0.1% glutaraldehyde in sodium acetate buffer, pH 6, for 2 min, followed by 1 h perfusion with ice-cold 2% paraformaldehyde and 0.1% glutaraldehyde in 0.1 M borate buffer, pH 9 (Kollo et al., 2008). After postfixation of the brain overnight in the second fixative, 70-μm-thick horizontal sections were cut with a vibrating microtome and stored in 0.1 M Na-phosphate buffer (pH 7.4). The sections were cryoprotected overnight in 30% sucrose and frozen/thawed three times with liquid nitrogen to enhance antibody penetration. Sections were then preincubated in 10% normal goat serum (NGS) in Tris-buffered saline (TBS), pH 7.4, for 3 hours at room temperature, followed by 5 days incubation at 4°C in primary antibodies (gephyrin/vGAT in combination with GFP) diluted in TBS, containing 5% NGS. Sections were then washed in TBS and incubated in secondary antibodies (Fab fragments) coupled to biotin (1:250; Jackson Immunoresearch) or to 1.4 nm colloidal gold particles (1:50; Nanoprobes Inc., Yaphank, NY) for 24 h. Ultrasmall gold particles were visualized with

the gold enhance-EM formulation (Nanoprobes) as described by the manufacturer. The sections were treated with 0.5% OsO4, and 1% uranyl acetate, dehydrated, and embedded in Epon 812. Ultrathin sections were collected on Nickel single-hole grids. Serial thin sections were cut in the EPL and GCL. eGFP-positive profiles were analysed in images taken from at least 6 sections at a magnification of 13,500x. They were observed and photographed in a JEM-1010 transmission electron microscope (Jeol, Japan) equipped with a side-mounted CCD camera (Mega View III, Soft Imaging System, Germany).

Statistical analyses

Data are presented as mean± SEM. Statistical analyses were made using one-way and two-way ANOVA, followed where appropriate by Tukey *post-hoc* tests (Prism software; GraphPad, version 6).

Results

Identification of adult-born GCs transduced by eGFP-gephyrin lentiviruses

Over-expression of gephyrin was achieved by injection of LVs encoding either rat gephyrin N-terminally fused to eGFP (eGFP-Geph), a phospho-deficient eGFP-gephyrin mutant, known to facilitate postsynaptic gephyrin clustering *in vitro* (eGFP-Geph(S270A)), or a dominant-negative mutant unable to form postsynaptic clusters (eGFP-Geph(L2B)) (see Introduction) into the rostral migratory stream of adult C57Bl6/J mice. As control, LV constructs expressing only eGFP or tdTomato were used. The eGFP fused to each gephyrin isoform allowed us to detect transfected GCs in the OB and to monitor their morphological development by fluorescence microscopy. Based on previous work (Pallotto et al., 2012; Panzanelli et al., 2009; Whitman and Greer, 2007), we followed their maturation between 14 and 90 dpi. For each gephyrin construct and time-point, tissue from 3-6 mice was used for analysis.

A first visual inspection of sections from LV-injected mice at early time-points revealed the presence of bright eGFP-Geph clusters in the GCL and EPL; however, it was difficult to trace the morphology of eGFP-Geph infected dendrites compared to the GFP-control GCs, which exhibited a uniform dendritic labeling (Fig. 1A-A''). GCs expressing eGFP-Geph(L2B) showed a weak, often undetectable fluorescence (data not shown). Hence, we enhanced the GFP signal in all subsequent experiments using immunohistochemistry allowing for better visualization of the cell soma, dendrites, and spines of transduced adult-born CGs (Fig. 2A-A'). To verify that the different eGFP-gephyrin isoforms fill up the entire GC, we co-injected a 1:1 mixture of two LVs encoding either eGFP-Geph(S270A) or eGFP-Geph(L2B) along with a LV expressing the red fluorescent protein tdTomato. At low magnification, we observed that GCs expressing eGFPGeph(S270A) (signal enhanced by immunofluorescence) exhibit a similar morphological development at 14 dpi compared to tdTomato-control cells (Fig. 1B), although they were distinctly less numerous, reflecting the difference in titer between the two LVs. Both cell populations had a branched apical dendrite penetrating the EPL. In contrast, GCs expressing eGFP-Geph(L2B) appeared different, having in most cases an unbranched apical dendrite that did not yet reach the EPL at 14 dpi (Fig. 1C). The difference in cell morphology gradually became more accentuated, as seen at 90 dpi, when eGFP-Geph(L2B)-positive dendrites had much fewer branches and spines (Fig. 2B-D) .

Examination of double-labeled cells at higher magnification confirmed that eGFP-Geph constructs filled up GCs to the same extent as tdTomato, revealing their morphology in detail and confirming that overexpression of the dominant-negative gephyrin L2B mutant impaired dendrite growth and spine formation (Fig. 1D-E). To further ensure that recombinant eGFP-gephyrin indeed reveals the entire cell, control experiments were performed by

iontophoretically loading eGFP-positive cells with Lucifer Yellow and examining them by dual immunofluorescence. Examination of double-labeled cells revealed a very strong Lucifer Yellow immunostaining and confirmed that eGFP-Geph labels all dendritic branches and spines, but not filopodia (Fig. 1F-F").

Taken together, these observations revealed that although the eGFP signal had to be amplified by immunolabeling for morphological analysis of transduced adult-born GCs, eGFP-gephyrin is not restricted to postsynaptic sites but fills the entire cell, except for filopodia. As GCs are axonless, we could not determine whether eGFP-gephyrin would also be transported into this subcellular compartment.

Differential alteration in dendrite development

We quantified dendrite arborization in GCs expressing the various gephyrin constructs at three distinct time-points to capture their maturation process (Fig. 2E-G). The number of terminal branches and total dendritic length were significantly different over time ($F_{Branches(2.426)}$ = 6.833, P = 0.0012; $F_{Length(2.450)}$ = 14.47, P<0.0001), depending on the gephyrin construct ($F_{Branches(3.426)}$ = 102.9, P<0.001; $F_{Length(3.450)}$ = 125.5, P<0.0001), but no interaction between these two factors was observed. Thus, eGFP-Geph(S270A) overexpression increased the number of terminal branches compared to eGFP-Geph at 21 and 90 dpi, without affecting total dendritic length, whereas eGFP-Geph(L2B) overexpression significantly reduced dendritic branching and length at all time-points analyzed (Fig. 2E-F).

In addition, using Sholl analysis to quantify dendritic complexity, we observed that overexpression of eGFP-Geph had no effect compared to eGFP-only (Fig. 2G), whereas dendrites of GCs expressing eGFP-Geph(L2B) were much shorter and less complex (one-way ANOVA; 14 dpi: $F_{(3,160)}$ = 9.175, P<0.0001; 21 dpi: $F_{(3,160)}$ = 8.942, P<0.0001; 90 dpi: $F_{(3,160)}$ = 4.93, P<0.01). Expression of eGFP-Geph(S270A) mutant, which favors the formation of GABAergic synapses *in vitro*, caused no significant overall differences compared to control cells at any time-point, except that dendritic arborization was transiently more complex when entering the EPL (Fig. 2G; one-way ANOVA, $F_{(3,64)}$ = 57.94, P<0.0001).

Differential effect of gephyrin mutants on neuronal survival

Given the strong effects of gephyrin mutants, notably Geph(L2B), on adult-born GC development, we wondered whether disrupting gephyrin scaffold formation might influence cell survival. Hence, we evaluated cell survival by quantifying the ratio of green/red cells at 14 and 90 dpi in mice co-injected with two LVs (tdTomato and eGFP-Geph(S270A) or eGFP-Geph(L2B); N=5-7 mice/group). The higher titer of the tdTomato LV resulted in more red cells compared to green cells at both 14 and 90 dpi. However, 47-50% of green cells were

also double-labeled with tdTomato, allowing us to analyze relative increase in green and yellow cells compared to red alone cells over time. tdTomato-positive GCs increased in number between 14 and 90 dpi (Table 2), suggesting that the residual LV, despite being replication-deficient, continuously transduced neuronal progenitors migrating through the rostral migratory stream. Hence, tdTomato-positive GCs seen at 90 dpi are all not of uniform age. We observed the similar phenomenon with eGFP-Geph(S270A) and eGFP-Geph(L2B) LVs. Importantly, the time-dependent increase eGFP-Geph(S270A)-positive cells was proportionally the same as for tdTomato-positive GCs at 90 dpi (>3-fold), indicating that their net survival rate was similar. However, when comparing eGFP-Geph(L2B)/tdTomato infected GCs, we found the ratio to be markedly reduced at 90 dpi compared to 14 dpi (Table 2), indicating that disruption of gephyrin scaffolding curtails the survival of adult-born GCs.

To further explore when survival is affected, we modeled survival curves to test the impact of either early mortality (up to 14 dpi; prior to synaptogenesis) or late mortality (after 21 dpi; due to failure of synaptic integration) (Fig. 3A-C). The best fit with the experimental data was obtained when both early and late mortality rates of GCs expressing eGFP-Geph(L2B) are increased 2-3 fold compared to tdTomato. These data allowed calculating the life-expectancy of newborn GCs, showing a marked reduction in cells expressing eGFP-Geph(L2B) (Fig. 3B-C). Therefore, this result implies that the age-distribution of eGFP-geph(L2B) expressing GCs at 90 dpi is altered compared to GCs marked with tdTomato, with a strong increase the fraction of young cells (Fig. 3D). To verify this prediction, we stained for DCX, a marker present in young, but not mature, adult-born GCs. At 14 dpi, the fraction of DCX-positive cells was not different between the three groups (42-50%); however, at 90 dpi, twice as many GCs transduced with eGFP-Geph(L2B) were positive for DCX (33%) compared to eGFP-Geph(S270A) (17%), or tdTomato (19%) (Fig. 3E-F).

We also measured radial migration of adult-born GCs into the OB to determine whether this parameter would be influenced by gephyrin mutations (Table 2). There was no significant difference between the three LVs analyzed at either 14 or 90 dpi, but a significant effect of time (eGFP(S270A): $F_{(1,12)} = 42.57$; $P<0.0001$; eGFP(L2B): $F_{(1,14)} = 72.37$, $P<0.0001$), indicating that migration into the granule cell layer (GCL) lasts for several weeks independently of the gephyrin construct overexpressed. This conclusion stands out when considering the migration distance relative to the width of the GCL; the fraction covered by migrating GCs increased by 25% from 40% at 14 dpi to 50% of the total GCL width at 90 dpi (Table 2).

Gephyrin-dependent modulation of spine formation

Next, we investigated the influence of gephyrin on spine formation on the apical dendrites of adult-born GCs. GCs have unusual spine heterogeneity. In the GCL, spines are innervated by glutamatergic terminals, whereas in the EPL, spines form reciprocal synapses with the dendrites of principal cells. In addition, in immature GCs, spines are also transient sites for GABAergic inputs along the entire apical dendrite (Panzanelli et al., 2009). Accordingly, it is conceivable that gephyrin modulates spine formation, as we observed here that eGFP-gephyrin constructs distinctly label spines in both immature and mature adult-born GCs (Fig. 4A-B).

In the GCL, quantification of spine density revealed a significant effect of time ($F_{(2, 395)}$ = 7.044, P = 0.001) and gephyrin construct ($F_{(3, 395)}$ = 80.16, P<0.0001), but no interaction ($F_{(6, 395)}$ = 0.3620, P = 0.9027) (Fig. 4C). eGFP-Geph expression caused no effect compared with eGFP, indicating that gephyrin overexpression by itself does not influence spine formation. In contrast, GCs expressing eGFP-Geph(S270A) exhibited a significant increase in spine density already at 14 dpi that persisted up to 90 dpi (Fig. 4C), suggesting that eGFP-Geph(S270A) facilitates spine formation. Finally, overexpression of eGFP-Geph(L2B) induced a clear deficit in spines on apical dendrites, evident at each of the time-points analyzed compared to control (Fig. 4C).

In the EPL, a significant effect of time ($F_{(2, 418)}$ = 4.982, P = 0.0073), gephyrin construct ($F_{(3,418)}$ = 126.9, P<0.0001), and interaction ($F_{(6, 418)}$ = 5.704, P<0.0001) was likewise observed. Again, overexpression of eGFP-Geph had no effect on spine density compared to eGFP (Fig. 4D), whereas eGFP-Geph(S270A) caused a net increase in spine density at all time-points. Expectedly, GCs expressing eGFP-Geph(L2B) had few spines in the EPL. However, a gradual increase occurred over time (Fig. 4D), suggesting that mature cells form reciprocal synapses with mitral cell dendrites.

Presence of postsynaptic α2-GABA$_A$Rs on spines

The presence of eGFP-Geph and eGFP-Geph(S270A) clusters in many spines of adult-born GCs was intriguing, considering that spines are either postsynaptic to glutamatergic inputs, or presynaptic to mitral cells. To determine whether eGFP-Geph-positive spines are indeed postsynaptic to GABAergic input, we used triple-staining for GFP, GABA$_A$R α2 subunit, and vesicular GABA transporter (vGAT; to label presynaptic terminals). The quantitative analysis showed that α2 subunit clusters are located on both apical dendritic shafts and spines in the GCL and EPL (Fig. 5, Table 3).

In the GCL, α2 subunit cluster density on dendritic shafts was dependent on time (two-way ANOVA; $F_{(2.399)}$ = 113.6, P<0.0001) and gephyrin construct ($F_{(3, 399)}$ = 880.4, P<0.0001), with a significant interaction ($F_{(6, 399)}$ = 17.20, P<0.0001). eGFP-Geph(L2B)-positive GCs had

much fewer α2 subunit clusters (Fig. 5A, Table 3) compared to all other constructs. In spines, there was likewise a significant effect of time ($F_{(2, 402)}$ = 68.3, *P*<0.0001), gephyrin construct ($F_{(3, 402)}$ = 2100, *P*<0.0001), and interaction ($F_{(6, 402)}$ = 64.77, *P*<0.0001) (Fig. 5B, Table 3). eGFP-Geph(S270A) expression caused a 2-5 fold increase in α2 subunit clusters compared to control, particular at 90 dpi, whereas eGFP-Geph(L2B) had a marked negative effect. Overall, about 25-30% of α2 subunit clusters were located in spines in the GCL (Fig. 5A-B, Table 3), a proportion similar to that reported previously in immature GCs at 3-7 dpi (Panzanelli et al., 2009), implying that expression of eGFP-Geph(S270A) favors the formation of immature spines. However, these spines are most likely transient, since the density of GABAergic synapses on the shaft did not increase over time.

In the EPL, the density of α2 subunit clusters on dendritic shafts varied little over time and among the constructs analyzed, except for GCs expressing eGFP-Geph(L2B), in which it gradually increased to control levels by 90 dpi (Fig. 5C, Table 3; two-way ANOVA; $F_{(6, 259)}$ = 41.88, *P*<0.0001). In spines, α2 subunit clusters are unlikely to be present in reciprocal synapses with mitral cell dendrites. Accordingly, the density of spines containing the α2 subunit was very low, except for the eGFP-Geph(S270A) construct, where they represented up to 50% of all α2 subunit clusters (Fig. 5D, Table 3). Therefore, eGFP-geph(S270A) favors the formation of GABAergic synapses on spines, albeit short-lived, as they are not efficiently converted into GABAergic synapses on the shaft. Conversely, expression of eGFP-Geph(L2B) virtually abolished the ability of GCs to form such GABAergic synapses on spines, whereas the formation of α2 subunit-negative spines, likely representing regular reciprocal synapses, was only partially impaired. Quantification confirmed our observations, as we found a significant effect of time ($F_{(2, 248)}$ = 123.3, *P*<0.0001), gephyrin construct ($F_{(3, 248)}$ = 731.1, *P*<0.0001), and interaction between these factors ($F_{(6, 248)}$ = 32.68, *P*<0.0001).

Analysis of high magnification 3D images in the GCL and EPL revealed that α2 subunit clusters on spines and shafts were typically apposed to vGAT-positive terminals (Fig. 5E, G, H), confirming their postsynaptic nature. Further, staining for vGLUT1 showed that GFP-positive spines negative for the α2 subunit were apposed to terminals containing vGLUT1, a marker of glutamatergic transmission (Fig. 5F).

GC ultrastructure is not altered by over-expression of eGFP-gephyrin constructs

The results so far revealed that eGFP-gephyrin constructs label all spines of adult-born GCs, either diffusely or by forming a bright fluorescent cluster. While gephyrin clusters in the spines often were co-localized with the α2-subunit, presumably forming transient GABAergic synapses, we wondered whether eGFP-gephyrin is also present in spines receiving glutamatergic synapses or in spines engaged in dendro-dendritic connections in the EPL.

Therefore, we used double immuno-labeling electron microscopy (EM) with antibodies against GFP and either gephyrin (mAb7a) or vGAT to analyze the ultrastructure of eGFP-positive spines, and notably the formation of GABAergic and reciprocal synapses. Analysis of GCs transduced with eGFP-Geph showed that the intensity of the GFP immuno-labeling was much stronger in the GCL than EPL, where it was barely detectable. Nevertheless, we readily observed in the GCL the presence of labeled profiles making (Fig. 6A1, 6A2) or receiving a GABAergic synapse (Fig. 6A3), some of which contained a prominent gephyrin immuno-labeling (Fig. 6A1, A3). In the EPL, all eGFP-positive spines observed were either presynaptic to a gephyrin-positive mitral cell profile (Fig. 6A4), or were forming a reciprocal synapse and, therefore, were postsynaptic to glutamatergic input (Fig. 6A5). Despite extensive sampling, we did not observe any GFP-positive profile postsynaptic to GABAergic input; in part, this might be due to the weak overall GFP labeling, possibly leading to many false-negative GC spine profiles.

Similar observations were made in images from GCs transduced with the eGFP-Geph(S270A) LV. Fig. 6B1-B1' illustrates an example of GFP-positive profile receiving a gephyrin-labeled GABAergic synapse; Fig. 6B2-B3 provide two examples of VGAT-GFP double-labeling, postsynaptic to unlabeled, presumably glutamatergic terminals. In the EPL, we again observed that eGFP-positive profiles were all either presynaptic, forming gephyrin-immunoreactive GABAergic synapses with mitral cell profiles (Fig. 6B4-5), or forming reciprocal synapses containing both a GABAergic and a glutamatergic synapse in the same profile (Fig. 6B6).

Finally, no distinct ultrastructural alteration was seen in GCs expressing eGFP-Geph(L2B). Very few postsynaptic eGFP-positive profile could be found in either the GCL or EPL, in line with the paucity of synapses received by these cells. Figure 6C1-C1' illustrates a rare example of a GFP-positive profile in the GCL, being postsynaptic to an unlabeled, presumably glutamatergic terminal. Unexpectedly, synapses formed by GFP-positive profiles in the GCL had a rather prominent postsynaptic density, which lacked gephyrin immunolabeling (Fig. 6C3-C4), although gephyrin immunogold labeling was detectable in their vicinity. In the EPL, eGFP-Geph(L2B)-positive profiles formed characteristic GABAergic and reciprocal synapses with mitral cell dendritic profiles, prominently immunopositive for gephyrin (Fig. 6C4-C5). Altogether, these results confirm that the presence of eGFP-gephyrin in spines cannot be taken as evidence for postsynaptic clusters in GABAergic synapses. Further, it does not affect apparently themorphological and ultrastructural differentiation of spines, notably thee formation of reciprocal synapses with the dendrites of principal cells.

Discussion

The results demonstrate that formation of GABAergic synapses containing a postsynaptic gephyrin scaffold is crucial for morphological differentiation, synaptic integration, and long-term survival of adult-born OB GCs. Remarkably, eGFP-Geph overexpression had almost no detectable effect, indicating that it does not interfere with neuronal differentiation and GABAergic synapse formation. In contrast, overexpression of phospho-deficient eGFP-Geph(S270A) favored dendritic branching and formation of transient GABAergic synapses on spines, containing α2-$GABA_A$Rs. This observation suggests that gephyrin phosphorylation at Ser270 is a mechanism limiting structural plasticity in both immature and mature GCs and implicates specific signaling pathways in the control of neuronal development. Finally, overexpression of eGFP-Geph(L2B), a gephyrin mutant unable to self-aggregate, largely impaired dendritic growth and branching, as well as formation of transient GABAergic synapses on spines. While this effect might be due to defective GABAergic transmission, we favor the view that it reflects the absence of signaling molecules anchored to the gephyrin scaffold, such as collybistin (Kins et al., 2000) and other gephyrin interactors that modulate the actin cytoskeleton (Maas et al., 2009) and thereby spine formation and dendrite branching. Since spines of adult-born GCs eventually become recipient of glutamatergic synapses in both the GCL and the EPL, a deficit in spine formation likely causes reduced excitatory transmission and its associated Ca^{++} signaling, further having an impact on neuronal differentiation (Kelsch et al., 2012). This cascade might eventually curtail long-term neuronal survival.

eGFP-Geph overexpressed in adult-born GCs not only forms postsynaptic clusters, but also accumulates in spines forming reciprocal synapses and being postsynaptic to glutamatergic axon terminals, as demonstrated ultrastructurally. In addition, when amplified by immunofluorescence, diffuse eGFP-Geph was detectable throughout the cell, except in filopodia. These observations indicate that gephyrin might have additional functions in neurons and that specific mechanisms are operant to ensure its selective clustering in GABAergic postsynaptic densities, while preventing its aggregation in other subcellular compartments. The numerous post-translational modifications of gephyrin provide potential molecular substrate underlying selective aggregation at GABAergic (and glycinergic) postsynaptic sites (Dejanovic and Schwarz, 2014; Dejanovic et al., 2014; Tyagarajan and Fritschy, 2014). The failure of eGFP-Geph(L2B) to form postsynaptic clusters underscores the importance of the surface-exposed loop encoded in this sequence. Remarkably, the L2B mutation disrupts a consensus site for binding to protein phosphatase 1, potentially implicating this site in the structural deficit preventing gephyrin clustering.

The need of immunofluorescence amplification in cells transduced with eGFP constructs precluded an electrophysiological analysis of single-transfected cells. Therefore, we were

not able to verify whether the changes in structural plasticity seen upon overexpression of gephyrin constructs were due to alterations in GABAergic synaptic transmission. Overcoming this pitfall will be necessary to determine the respective role of GABAergic synaptic function and of down-stream signaling cascades depending on gephyrin clustering for proper GC differentiation and survival.

Significance of the gephyrin S270A point-mutation

Ser270 is among the best characterized gephyrin residues that are phosphorylated *in vivo*. Abolishing its phosphorylation by point-mutation or blocking the activity of GSK3β leads to the formation of supernumerary gephyrin clusters in cultured neurons, as well as an increase in dendritic growth and branching, accompanied by enhanced GABAergic synaptic transmission (Kuhse et al., 2012; Rui et al., 2013; Tyagarajan et al., 2013; Tyagarajan et al., 2011). While the underlying mechanism is not clarified, GABAergic transmission was shown to regulate dendritic growth, in association with a higher stability of microtubules (Gascon et al., 2006). Our results imply that gephyrin phosphorylation modulates its capacity to interact with (or activate) molecules involved in synaptogenesis and dendritic growth. Remarkably, however, there was no overall increase in spine density over time in transfected GCs (Fig. 5), although they have a higher density of spines containing the α2-subunit than control cells in both the GCL and EPL. For this reason, we conclude that eGFP-Geph(S270A) favors the formation of transient, short-lived spines, as seen in immature cells. Therefore, *in vivo*, homeostatic mechanisms likely exist, which limit the formation of supernumerary spines in adult-born GCs. Likewise, quantification of α2-subunit clusters on dendritic shafts of GCs expressing eGFP-Geph(S270A) showed no increase over time, confirming a possible homeostatic regulation. Taken together, these findings indicate that eGFP-Geph(S270A) may have the ability to keep the cell in a state of plasticity normally restricted to initial phases of maturation (Kelsch et al., 2009; Pallotto et al., 2012; Whitman and Greer, 2007).

Consequences of preventing post-synaptic gephyrin clustering

In the Geph(L2B) mutant, 8 out of 10 residues (DIDGVRKI) forming a surface-exposed loop in the E-domain of rat gephyrin were replaced by their homologues from bacterial MoeA (KL..SNSW). As a consequence, gephyrin aggregation is severely impaired. Remarkably, replacing only 6 residues (IDGVRK) by their homologues (L..SNS) strongly increases the aggregation propensity of gephyrin, leading to formation of supernumerary postsynaptic clusters (Lardi-Studler et al., 2007). Neither mutation affects the Moco synthesis activity of gephyrin, suggesting that this surface-exposed loop, which is poorly conserved phylogenetically, is a key regulator of postsynaptic gephyrin function. While the L2B mutation is dominant-negative, we observed the formation of a few gephyrin clusters colocalized with

the α2 subunit, as previously reported *in vitro*. Accordingly, overexpression of eGFP-Geph(L2B) might not fully abolish synaptic GABAergic function. Nevertheless, the consequences on the structural development and survival of adult-born GCs were stronger than after abolition of α2-$GABA_A$Rs (Pallotto et al., 2012), indicating that interfering with postsynaptic gephyrin clustering has pronounced detrimental effects during neuronal development. The long-term effectsinclude limited life-span of GCs overexpressing eGFP-Geph(L2B), implying that at 90 dpi, this cell population comprises a large fraction of young cells with reduced, or possibly slow maturation (Fig. 3D), contributing to the deficit in dendrite length and branching, and reduced spine density seen at all time-points examined. It is unlikely, however, that slow maturation alone explains the dramatic morphological phenotype of these cells. Rather, the impairment of dendritic growth and spine formation might be related to defective synaptic integration and appropriate downstream signaling. It is noteworthy that dendrite and spine profiles appeared unaltered ultrastructurally, and reciprocal synapses could readily be detected in the EPL at 21 dpi. Therefore, the eGFP-Geph(L2B) mutation severely limits the ability of cells to form transient GABAergic synapses on spines, opposite to the phenotype of eGFP-Geph(S270A). Consequently, it is this "plasticity deficit" rather than a "structural deficit" that negatively affects the formation of spines and dendritic branching.

Signaling at the gephyrin scaffold

There are at least two possible mechanisms explaining the opposite phenotype of GCs expressing eGFP-Geph(S270A) and eGFP-Geph(L2B). First, given that gephyrin interacts with numerous signaling molecules (see Introduction), failure to form a postsynaptic scaffold might affect downstream signaling contributing to remodeling of the cytoskeleton and spine formation. In particular, the control of the small GTPases cdc-42 and TC-10 activity by gephyrin-collybistin interaction (Mayer et al., 2013; Papadopoulos et al., 2007) is an obvious candidate. Second, reduced spinogenesis limits the formation of afferent synapses onto adult-born GCs, both GABAergic and glutamatergic. Both types of synapses might generate depolarizing signals, notably in immature cells, leading to activation of NMDA receptors (Kelsch et al., 2012) and opening of voltage-dependent Ca^{++} channels. Ca^{++} contributes to activation of protein kinases and phosphatases, including CaMKII and calcineurin, activating downstream signaling cascades and transcription factors, in particular CREB, which is necessary for maturation and survival of newborn neurons (Jagasia et al., 2009; Obrietan et al., 2002) and their morphological differentiation (Giachino et al., 2005; Herold et al., 2011). Additional mechanisms possibly include Ca^{++}-dependent activation of calpain, a neuron-specific protease that regulates a vast array of synaptic and structural proteins and modulates gephyrin postsynaptic clustering (Tyagarajan et al., 2011). Therefore, the focus of

future work will be to elucidate how gephyrin scaffolds modulate spine formation, in particular at immature stages when newborn cells still receive only limited glutamatergic input.

In conclusion, the present work uncovers a key role of gephyrin as a scaffolding molecule in GABAergic postsynaptic densities for modulating structural plasticity in developing neurons, thereby expanding the repertoire through which the GABAergic system regulates neuronal development and maturation.

Acknowledgements: We are grateful to Dr. Sebastian Jessberger for the gift of virus plasmids, Dr. P.-M. Lledo and collaborators for the gift of tdTomato lentivirus, Dr. Steven Brown for providing reagents for lentivirus production, Dr. Venceslas Duveau, Dr. Ludmila Gášpár, Claire deGroot, Christine Muheim, and Dennis Mircsof for help with production of lentiviruses, Dr. Laszlo Vutskits for support and advice with the Lucifer Yellow experiment, and Dr. C. Lafourcade for help with experiments and scientific support.

Author contributions: Study concept and design: JMF, SKT. Acquisition of data: FD, MP, FV, MG, PP. Analysis and interpretation of data: FD, MP, PP, JMF. Drafting of the manuscript: FD. Critical revision of the manuscript for important intellectual content: all co-authors. Statistical analysis: FD. Obtained funding: MP, MG, JMF. Administrative, technical, and material support: MAV. Study supervision: JMF.

Conflict of interest: The authors have no conflict of interest to declare.

References

Bellocchio EE, Reimer RJ, Fremeau RT, Jr., Edwards RH. 2000. Uptake of glutamate into synaptic vesicles by an inorganic phosphate transporter. Science 289:957-960.

Bovetti S, Gribaudo S, Puche A, De Marchis S, Fasolo A. 2011. From progenitors to integrated neurons: role of neurotransmitters in adult olfactory neurogenesis. J Chem Neuroanat 42:304-316.

Brünig I, Suter A, Knuesel I, Luscher B, Fritschy JM. 2002. GABAergic presynaptic terminals are required for postsynaptic clustering of dystrophin, but not of $GABA_A$ receptors and gephyrin. J Neurosci 22:4805-4813.

Dejanovic B, Schwarz G. 2014. Neuronal nitric oxide synthase-dependent S-nitrosylation of gephyrin regulates gephyrin clustering at GABAergic synapses. J Neurosci 34:7763-7768.

Dejanovic B, Semtner M, Ebert S, Lamkemeyer T, Neuser F, Lüscher B, Meier J, Schwarz G. 2014. Palmitoylation of gephyrin controls receptor clustering and plasticity of GABAergic synapses. PLoS Biol 12:e1001908.

Dumoulin A, Rostaing P, Bedet C, Levi S, Isambert MF, Henry JP, Triller A, Gasnier B. 1999. Presence of the vesicular inhibitory amino acid transporter in GABAergic and glycinergic synaptic terminal boutons. J Cell Sci 112:811-823.

Fujiyama F, Furuta T, Kaneko T. 2001. Immunocytochemical localization of candidates for vesicular glutamate transporters in the rat cerebral cortex. J Comp Neurol 435:379-387.

Gascon E, Dayer AG, Sauvain MO, Potter G, Jenny B, De Roo M, Zgraggen E, Demaurex N, Muller D, Kiss JZ. 2006. GABA regulates dendritic growth by stabilizing lamellipodia in newly generated interneurons of the olfactory bulb. J Neurosci 26:12956-12966.

Ge S, Goh EL, Sailor KA, Kitabatake Y, Ming GL, Song H. 2006. GABA regulates synaptic integration of newly generated neurons in the adult brain. Nature 439:589-593.

Ge S, Pradhan DA, Ming GL, Song H. 2007. GABA sets the tempo for activity-dependent adult neurogenesis. Trends Neurosci 30:1-8.

Giachino C, De Marchis S, Giampietro C, Parlato R, Perroteau I, Schütz G, Fasolo A, Peretto P. 2005. cAMP response element-binding protein regulates differentiation and survival of newborn neurons in the olfactory bulb. J Neurosci 25:10105-10118.

Herold S, Jagasia R, Merz K, Wassmer K, Lie D. 2011. CREB signalling regulates early survival, neuronal gene expression and morphological development in adult subventricular zone neurogenesis. Mol Cell Neurosci 46:79-88.

Jagasia R, Steib K, Englberger E, Herold S, Faus-Kessler T, Saxe M, Gage FH, Song H, Lie DC. 2009. GABA-cAMP response element-binding protein signaling regulates maturation and survival of newly generated neurons in the adult hippocampus. J Neurosci 24:7966-7977.

Kelsch W, Li Z, Eliava M, Goengrich C, Monyer H. 2012. GluN2B-containing NMDA receptors promote wiring of adult-born neurons into olfactory bulb circuits. J Neurosci 32:12603-12611.

Kelsch W, Lin C, Mosley C, Lois C. 2009. A critical period for activity-dependent synaptic development during olfactory bulb adult neurogenesis. J Neurosci 29:11852-11858.

Kins S, Betz H, Kirsch J. 2000. Collybistin, a newly identified brain-specific GEF, induces submembrane clustering of gephyrin. Nature Neurosci 3:22-29.

Kuhse J, Kalbouneh H, Schlicksupp A, Mükusch S, Nawrotzki R, Kirsch J. 2012. Phosphorylation of gephyrin in hippocampal neurons by cyclin-dependent kinase CDK5 at Ser-270 is dependent on collybistin. J Biol Chem 287:30952-30966.

Lagier S, Panzanelli P, Russo RE, Nissant A, Bathellier B, Sassoè-Pognetto M, Fritschy JM, Lledo PM. 2007. GABAergic inhibition at dendrodendritic synapses tunes γ oscillations in the olfactory bulb. Proc Natl Acad Sci USA 104:7259-7264.

Lardi-Studler B, Smolinsky B, Petitjean CM, Koenig F, Sidler C, Meier JC, Fritschy JM, Schwarz G. 2007. Vertebrate-specific sequences in the gephyrin E-domain regulate cytosolic aggregation and postsynaptic clustering. J Cell Biol 120:1371-1382.

Ledergerber DA, Fritschy JM, Kralic JE. 2006. Impairment of dentate gyrus neuronal progenitor cell differentiation in a mouse model of temporal lobe epilepsy. Exp Neurol 199:130-142.

Lepousez G, Valley M, Lledo P. 2013. The impact of adult neurogenesis on olfactory bulb circuits and computations. Annu Rev Physiol 75:339-363.

Lledo PM, Alonso A, Grubb MS. 2006. Adult neurogenesis and fuctional plasticity in neuronal circuits. Nature Rev Neurosci 7:179-193.

Maas C, Belgardt D, Lee H, Heisler F, Lappe-Siefke C, Magiera M, van Dijk J, Hausrat T, Janke C, Kneussel M. 2009. Synaptic activation modifies microtubules underlying transport of postsynaptic cargo. Proc Natl Acad Sci USA 106:8731-8736.

Mayer S, Kumar R, Jaiswal M, Soykan T, Ahmadian M, Brose N, Betz H, Rhee J, Papadopoulos T. 2013. Collybistin activation by GTP-TC10 enhances postsynaptic gephyrin clustering and hippocampal GABAergic neurotransmission. Proc Natl Acad Sci USA 110:20795-20800.

Ming G, Song H. 2011. Adult neurogenesis in the mammalian brain: significant answers and significant questions. Neuron 70:687-702.

Nissant A, Pallotto M. 2011. Integration and maturation of newborn neurons in the adult olfactory bulb--from synapses to function. Eur J Neurosci 33:1069-1077.

Notter T, Panzanelli P, Pfister S, Mircsof D, Fritschy J. 2014. A protocol for concurrent high-quality immunohistochemical and biochemical analyses in adult mouse central nervous system. Eur J Neurosci 39:165-175.

Obrietan K, Gao XB, Van Den Pol AN. 2002. Excitatory actions of GABA increase BDNF expression via a MAPK-CREB-dependent mechanism--a positive feedback circuit in developing neurons. J Neurophysiol 88:1005-1015.

Pallotto M, Deprez F. 2014. Regulation of adult neurogenesis by GABAergic transmission: signaling beyond $GABA_A$-receptors. Front Cell Neurosci 8:166.

Pallotto M, Nissant A, Fritschy JM, Rudolph U, Sassoè-Pognetto M, Panzanelli P, Lledo PM. 2012. Early formation of GABAergic synapses governs the development of adult-born neurons in the olfactory bulb. J Neurosci 32: 9103-9115.

Panzanelli P, Bardy C, Nissant A, Pallotto M, Sassoè-Pognetto M, Lledo PM, Fritschy JM. 2009. Early synapse formation in developing interneurons of the adult olfactory bulb. J Neurosci 29:15039-15052.

Panzanelli P, Gunn BG, Schlatter MC, Benke D, Tyagarajan SK, Scheiffele P, Belelli D, Lambert JJ, Rudolph U, Fritschy JM. 2011. Distinct mechanisms regulate $GABA_A$ receptor and gephyrin clustering at perisomatic and axo-axonic synapses on CA1 pyramidal cells. J Physiol 589:4959-4980.

Papadopoulos T, Korte M, Eulenburg V, Kubota H, Retiounskaia M, Harvey RJ, Harvey K, O'sullivan GA, Laube B, Hulsmann S, Geiger JR, Betz H. 2007. Impaired GABAergic transmission and altered hippocampal synaptic plasticity in collybistin-deficient mice. EMBO J 26:3888-3899.

Platel JC, Lacar B, Bordey A. 2007. GABA and glutamate signaling: homeostatic control of adult forebrain neurogenesis. J Mol Histol 38:602-610.

Rui Y, Myers K, Yu K, Wise A, De Blas A, Hartzell H, Zheng J. 2013. Activity-dependent regulation of dendritic growth and maintenance by glycogen synthase kinase 3β. Nature Commun 4:2628.

Sassoè-Pognetto M, Panzanelli P, Sieghart W, Fritschy JM. 2000. Co-localization of multiple $GABA_A$ receptor subtypes with gephyrin at postsynaptic sites. J Comp Neurol 420:481-498.

Todd AJ, Hughes DI, Polgar E, Nagy GG, Mackie M, Ottersen OP, Maxwell DJ. 2003. The expression of vesicular glutamate transporters VGLUT1 and VGLUT2 in neurochemically defined axonal populations in the rat spinal cord with emphasis on the dorsal horn. Eur J Neurosci 17:13-27.

Tyagarajan S, Ghosh H, Yévenes G, Imanishi S, Zeilhofer H, Gerrits B, Fritschy J. 2013. Extracellular signal-regulated kinase and glycogen synthase kinase 3β regulate gephyrin postsynaptic aggregation and GABAergic synaptic function in a calpain-dependent mechanism. J Biol Chem 288:9634-9647.

Tyagarajan SK, Fritschy JM. 2014. Gephyrin, a master regulator of neuronal function? Nature Rev Neurosci 15:141-156.

Tyagarajan SK, Ghosh H, Yevenes GE, Nikonenko I, Ebeling C, Schwerdel C, Sidler C, Zeilhofer HU, Gerrits B, Muller D, Fritschy JM. 2011. Regulation of GABAergic synapse formation and plasticity by GSK3β-dependent phosphorylation of gephyrin. Proc Natl Acad Sci USA 108:379-384.

Whitman MC, Greer CA. 2007. Synaptic integration of adult-generated olfactory bulb granule cells: basal axodendritic centrifugal input precedes apical dendrodendritic local circuits. J Neurosci 27:9951-9961.

Whitman MC, Greer CA. 2009. Adult neurogenesis and the olfactory system. Prog Neurobiol 89:162-175.

Zeilhofer HR, Studler B, Arabadzisz D, Schweizer C, Ahmadi S, Layh B, Bösl MR, Fritschy JM. 2005. Glycinergic neurons expressing enhanced green fluorescent protein in bacterial artificial chromosome transgenic mice. J Comp Neurol 482:123-141.

Table 1: List of primary antibodies

Target protein	Species	Dilution	Source; catalog	RRID	Method
Doublecortin	Guinea pig	1:1000	Chemicon; AB2253	RRID:AB_1586992	IF
GFP	chicken	1:2000	Aves Laboratories; GFP-1020	RRID:AB_10000240	IF
	rabbit	1:700	Synaptic Systems; 132 002	RRID:AB_887725	EM
Gephyrin	mouse	1:1000	Synaptic Systems; mAb7a; 147011	RRID:AB_887717	IF, EM
$GABA_AR$ α2-subunit	Guinea pig	1:1000	Self-made; Fritschy and Mohler, 1995		IF
Lucifer Yellow	Rabbit	1:5000	Invitrogen, AB5750	RRID:AB_1501344	IF
vGAT	rabbit	1:3000	Synaptic Systems; 131 003	RRID:AB_887869	IF
vGAT	GP	1:10'000	Synaptic Systems; 131 004	RRID:AB_887869	EM
vGLUT1	rabbit	1:10'000	Synaptic Systems; 135 002	RRID:AB_2315546	IF

Abbreviations: EM, immuno-electron microscopy; IF, immunofluorescence

Table 2: Quantification of adult-born GCs for assessing their survival

A) Number of labeled neurons/section						
	LV mixture tdTomato – S270A			*LV Mixture tdTomato – L2B*		
	tdTomato	S270A	%	tdTomato	L2B	%
14 dpi	279±30	48±9	16.1	293±26	85±12	26.2
90 dpi	1057±114	165±17	14.6	1009±108	153±18	14.1
B) Migration distance from the rostral migratory stream in μm (and % GCL width)						
	LV mixture tdTomato – S270A			*LV Mixture tdTomato – L2B*		
	tdTomato		S270A	tdTomato		L2B
14 dpi	121±9	43	118±10	39	121±9	42	113±9	38
90 dpi	149±9	50	151±10	49	149±9	51	147±9	50

The number of GCs overexpressing tdTomato or eGFP-Geph constructs was determined at 14 and 90 dpi for assessing differences in survival rates and migration into the olfactory bulb. Values are mean±SEM number of cells/section (N=4-7 mice per group). The decreased fraction of eGFP-Geph(L2B)-positive cells at 90 dpi compared to 14 dpi indicates reduced survival.

Table 3: Number of α2-subunit clusters on dendrites and spines

GCL

α2-subunit clusters on shaft/ primary segment

	eGFP	eGFP-Geph	eGFP-Geph(S270A)	eGFP-Geph(L2B)
14 dpi	16.0±1.1	12.6±1.9	14.2±1.3	10.0±1.0
21 dpi	14.6±1.7	14.0±2.4	16.3±1.8	8.5±2.6
90 dpi	12.2±3.1	12.0±3.3	10.3±1.3	6.7±1.9

α2-subunit clusters on spines/ primary segment

	eGFP	eGFP-Geph	eGFP-Geph(S270A)	eGFP-Geph(L2B)
14 dpi	3.4±1.6	4.7±1.7	7.0±1.6	0.7±0.5
21 dpi	3.5±0.8	3.8±1.4	6.6±0.9	0.3±0.4
90 dpi	1.5±0.4	2.4±1.3	6.2±2.1	1.1±0.7

EPL

α2-subunit clusters on shaft/ apical dendrites in the EPL

	eGFP	eGFP-Geph	eGFP-Geph(S270A)	eGFP-Geph(L2B)
14 dpi	12.8±5.2	16.1±2.0	19.2±7.9	
21 dpi	21.0±3.3	24.5±4.4	23.9±4.7	2.4±1.2
90 dpi	21.9±1.0	20.7±1.1	19.9±4.8	10.1±2.2

α2-subunit clusters on spines/ apical dendrites in the EPL

	eGFP	eGFP-Geph	eGFP-Geph(S270A)	eGFP-Geph(L2B)
14 dpi	2.2±0.5	3.0±1.2	11.3±9.6	
21 dpi	2.2±2.1	4.1±3.3	13.9±3.5	0.0±0.0
90 dpi	4.3±1.4	5.0±0.5	18.4±1.6	0.7±0.7

Absolute cluster numbers were calculated based on average densities shown in Supporting Figure S4 and average length of dendrites shown in Figure 2.

Figure Legends

Figure 1

Identification of adult-born GCs transduced with eGFP and eGFP-gephyrin constructs. ***A-A".*** Appearance of GCs transduced with the constructs indicated and visualized by confocal laser scanning microscopy without eGFP-immunofluorescence. While eGFP diffusely filled the GC, eGFP-gephyrin constructs formed large aggregates and small clusters, but the morphology of the cell could not be recognized. ***B-C*****.** Low-magnification images showing the distribution and morphology of tdTomato- and eGFP-Geph(S270A)- or eGFP-Geph(L2B)-positive adult-born GCs at 14 dpi, as detected by immunofluorescence staining against GFP. While tdTomato-transduced cells were much more numerous, no obvious differences in distribution were observed. However, the apical dendrites of eGFP-Geph(L2B)-positive adult-born GCs appeared shorter and did not reach the EPL. ***D-E.*** Representative images of double-transduced adult-born GCs at 21 dpi with LVs encoding tdTomato (red) and eGFP-Geph(S270A) (green) or eGFP-Geph(L2B) (green), demonstrating that in both cases the eGFP-tagged proteins can be detected by immunofluorescence in the entire cell (yellow in **D"** and **E"**). Note the paucity of spines in the GC transduced with eGFP-Geph(L2B). ***F-F".*** Example of an eGFP-Geph-positive GC dendrite (green) filled with Lucifer Yellow (red) at 21 dpi, showing double-labeling of dendritic shaft and spines (arrow), whereas filopodia contain no detectable eGFP-Geph immunofluorescence (stars). Scale bars: A, D, E, F, 10 μm; B-C, 100 μm.

Figure 2

Morphometric analysis of apical dendrite arborization of eGFP-gephyrin-transduced GCs. ***A-A'.*** Example of a cell visualized without (**A**, green) and with (**A'**, red) immunofluorescence for eGFP. Note that the eGFP-Geph construct fills the entire cells and forms local clusters recognized by their intense fluorescence staining. ***B.*** GC transduced with eGFP-Geph(S270A), exhibiting a spiny apical dendrite in the GCL that branches extensively upon entering in the EPL. ***C.*** Apical dendrite of a GC transduced with eGFP-Geph(L2B) that is largely devoid of spines in the GCL and forms only few branches in the EPL. ***D.*** Example of GC that migrated close to the mitral cell layer (MCL) and forms an apical dendrite with a single bifurcation in the EPL. ***E-F.*** Quantification of terminal branches and total dendritic length, represented by bar-graphs (mean±SEM; *N*=3-6 mice/group). **P*<0.05, ***P*<0.01, ****P*<0.001, *****P*<0.0001 compared to eGFP and eGFP-Geph; Tukey *post-hoc* tests). No significant difference over time was observed. ***C*****.** Quantification of apical dendritic arborization by Sholl analysis at 14, 21 and 90 dpi. The number of intersections between

eGFP-positive dendrite segments and virtual concentric lines centered on the cell body and spaced by 10 μm is depicted (mean±SEM; *N*=3-6 mice/group). For statistical comparison between groups, the area-under-the-curve was compared by one-way ANOVA at each time-point. No difference in dendritic complexity was observed, except for GCs expressing eGFP-Geph(L2B) (*P*<0.001 at each time-point). In addition, at 21 dpi, quantification of eGFP-Geph(S270A)-positive dendrites in the inner half of the EPL (between the two vertical lines) revealed a significant difference compared to eGFP and eGFP-Geph (*P*<0.05). Scale bars in A-D: 20 μm.

Figure 3

Effect of eGFP-Geph(S270A) and eGFP-Geph(L2B) over-expression on neuronal survival. ***A-D.*** Modeling data testing whether GCs transduced by eGFP-Geph(L2B) have a higher mortality rate initially (i.e. weeks 1-3, before differentiation) or late (i.e., weeks 4-12, after differentiation), or both. The model assumes three conditions: 1) continuous (but slowly declining) production of transduced GCs; 2) initially high, but rapidly declining mortality rate during weeks 1-3; 3) long-term low, but slowly raising mortality rate thereafter. **A.** Curves depicting the weekly evolution of the mortality rate of transduced GCs over time, depending on the initial and late mortality rate constants for tdTomato-positive GCs set to fit with the number of cells counted experimentally at 14 and 90 dpi (vertical bars); nearly identical time-constants apply for eGFP-Geph(S270A)-positive GCs. For eGFP-Geph(L2B)-positive cells, two scenario are depicted ($L2B_{low}$: initial mortality rate identical to tdTomato (33% per week); $L2B_{high}$: initial mortality rate doubled; in both cases, the late mortality rates have to be much higher than for tdTomato to reach the cell numbers seen at 90 dpi, suggesting that the eGFP-Geph(L2B) lentivirus limits the life-span of adult-born GCs. However, scenario $L2B_{low}$ is unlikely, because the late mortality rate reaches 100% at 12 weeks post-injection (arrow); therefore, this gephyrin mutant likely also affects the survival of non-differentiated GCs. ***B-C.*** Curves depicting the number of labeled GCs expected weekly based on the mortality rates shown in ***A***. For tdTomato and eGFP-Geph(S270A), the maximum is reached after 3 months, whereas for eGFP-Geph(L2B) it is reached at either 7.5 or 8.5 weeks; these data also allowed calculating the average life-span of GCs that had survived the first 3 weeks. Panel **D** depicts the age-distribution of adult-born GCs at 90 dpi, depending on their mortality rate. The number of GCs produced after the first week had to be set to 220 for tdTomato, 38 for eGFP-Geph(S270A), 70 for eGFP-Geph$(L2B)_{low}$, and 150 for eGFP-Geph$(L2B)_{high}$. A weekly rate of decline in production was set identically for all constructs (5%). Changing these parameters had little impact on the differential shape of the curves shown in panels B-D, but imposed to adjust the mortality rates accordingly. ***E.*** Fraction of GCs transduced with tdTomato, eGFP-Geph(S270A), or eGFP-Geph(L2B) that are positive for DCX at 14 and 90

dpi, confirming the higher fraction of immature cells in the latter group. ***F.*** Representative photomicrographs of DCX staining (blue) of adult-born GCs (arrowheads: tdTomato; arrows: eGFP-Geph(S270A)) at 14 and 90 dpi. Note the overall increase of tdTomato-positive cells between these two time points. Scale bar, 20 μm.

Figure 4

Quantification of spine density of adult-born GCs in the GCL and EPL. *A-B.* Representative images of spines on the apical dendrite of eGFP-positive GCs in the GCL (**A**) and EPL (**B**) at 21 dpi, illustrating that the majority of immuno-positive spines have a mature morphology and contain a prominent eGFP-gephyrin aggregate, except for eGFP-Geph(L2B). ***C-D.*** Quantification of spine density (mean±SEM; N=3-6 mice/group) on apical dendrites in the GCL (**C**) and EPL (**D**). eGFP-Geph(S270A)-positive GCs had a significant increased spine density, whereas eGFP-Geph(L2B)-positive GCs had a reduced spine density (**P*<0.05; ***P*<0.01; ****P*<0.001 ; *****P*<0.0001 compared to eGFP and eGFP-Geph; Tukey *post-hoc* test). Scale bars: ***A, B,*** 10 μm.

Figure 5

Synaptic integration of adult-born GCs in the GCL and EPL. *A, C.* Quantification of the density of α2 subunit clusters co-localized with eGFP on shafts at 14, 21 and 90 dpi in the GCL (**A**) and EPL (**C**) (mean±SEM; *N*=3-6 mice/group) (**P*<0.05; ***P*<0.01; ****P*<0.001; *****P*<0.0001 compared to eGFP; Tukey *post-hoc* test). ***B, D.*** Quantification of the density of eGFP-positive spines containing α2 subunit clusters co-localized with at 14, 21 and 90 dpi in the GCL (**B**) and EPL (**D**) (mean±SEM; *N*=3-6 mice/group) (***P*<0.01; *****P*<0.0001 compared to eGFP; Tukey *post-hoc* test). Comparison of these data with Fig. 4C-D reveals that the fraction of spines carrying an α2 subunit cluster is much lower in the EPL than GCL, in line with the predominance of reciprocal synapses on spines in the EPL. ***E.*** Triple immunofluorescence staining (3D projections depicted in the 3 Cartesian planes) for eGFP (green), α2 subunit (red) and vGAT (blue), depicting α2 subunit clusters on eGFP-Geph(S270A)-positive dendritic shafts (arrow) and spines (arrowhead) apposed to vGAT-immunofluorescent terminals in the GCL at 21 dpi. ***F.*** Triple immunofluorescence staining for eGFP (green), α2 subunit (red) and vGLUT1 (blue) showing that α2-subunit clusters in eGFP-Geph(S270A)-positive GCs dendritic shafts (arrow) and spines (arrowhead) are not apposed to vGLUT1-immunofluorescent terminals; whereas spines negative for the α2 subunit were often apposed to vGLUT1 terminals (stars). ***G-H.*** Double and triple immunofluorescence staining for eGFP (green), α2 subunit (red) and vGAT (blue) depicting

α2 subunit clusters on eGFP-Geph(S270A)-positive dendritic shafts (arrow) and spine-like structures (arrowhead) in the EPL at 21 dpi. Scale bars: ***E-H,*** 5 μm.

Figure 6

Double-labeling immunoelectron microscopy of adult-born GCs expressing eGFP-Geph (Fig. *6A*), eGFP-Geph(S270A) (Fig. *6B*), or eGFP-Geph(L2B) (Fig. *6C*) at 21 dpi.

Single- and double-labeled profiles were identified in the GCL and EPL and analyzed for their synaptic contacts. eGFP was detected by immunoperoxidase staining and either gephyrin (mAb7a) or vGAT by immunogold labeling. ***A1-A3***. eGFP-Geph-positive profiles (*) in the GCL making or receiving symmetric synapses that are either strongly labeled for gephyrin (**A1**, **A3**; arrow) or devoid of labeling (**A2**). ***A4-A5*.** Examples of GABAergic (A4) and reciprocal (A5) synapses between a mitral cell (MC) dendrite and eGFP-positive GC profile (*); the arrows point to gephyrin immunogold labeling; the arrowhead indicates the glutamatergic postsynaptic density. ***B1*-*B1'*.** Pair of consecutive sections depicting a presynaptic profile in the GCL making multiple symmetric synapses, some of which labeled for gephyrin (arrows) on a GC profile positive for eGFP-Geph(S270A) (*). ***B2-B3***. Double-labeled GC profiles in the GCL [eGFP-Geph(S270A) (*) and vGAT (#)] receiving a symmetric (**B2**) or an asymmetric (**B3**, arrowhead) synapse from immunonegative presynaptic profiles. ***B4-B4'.*** eGFP-Geph(S270A)-positive GC profile (*) making a reciprocal synapse with a mitral cell dendrite, as seen in two consecutive sections. The arrow points to gephyrin labeling and the arrowhead to the asymmetric postsynaptic density ***B5***. Example of labeled GC profile in the EPL (*) making a symmetric synapse strongly positive for gephyrin (arrows). ***B6***. Double-labeled GC profile, positive for GFP (*) and vGAT (#) forming a reciprocal synapse with a MC dendrite profile (arrowhead and arrow point to the asymmetric and symmetric postsynaptic density, respectively). ***C1*-*C4***. Examples of eGFP-Geph(L2B)-positive profiles (*) in the GCL making (**C1**, **C2**) or receiving (**C3**, **C3'**) synaptic contacts devoid of gephyrin labeling; in panels **C1** and **C2**, the postsynaptic density is unusually thick for being a GABAergic synapse; in **C3-C3'**, the GFP-positive profile receives a presumptive glutamatergic synapse (arrowheads). ***C4-C5*** Examples of eGFP-labeled profiles (*) in the EPL forming a symmetric synapse with a MC dendrite. Arrows point to gephyrin labeling postsynaptically. Scale bars: 0.5 μm.

Graphical abstract

Expression of eGFP-gephyrin in adult-born olfactory bulb granule cells (green) and the marker tdTomato (cyan) was used to test the role of GABAergic postsynaptic density proteins in the maturation and morphological differentiation of these neurons, which are constantly generated during adult life in rodents.

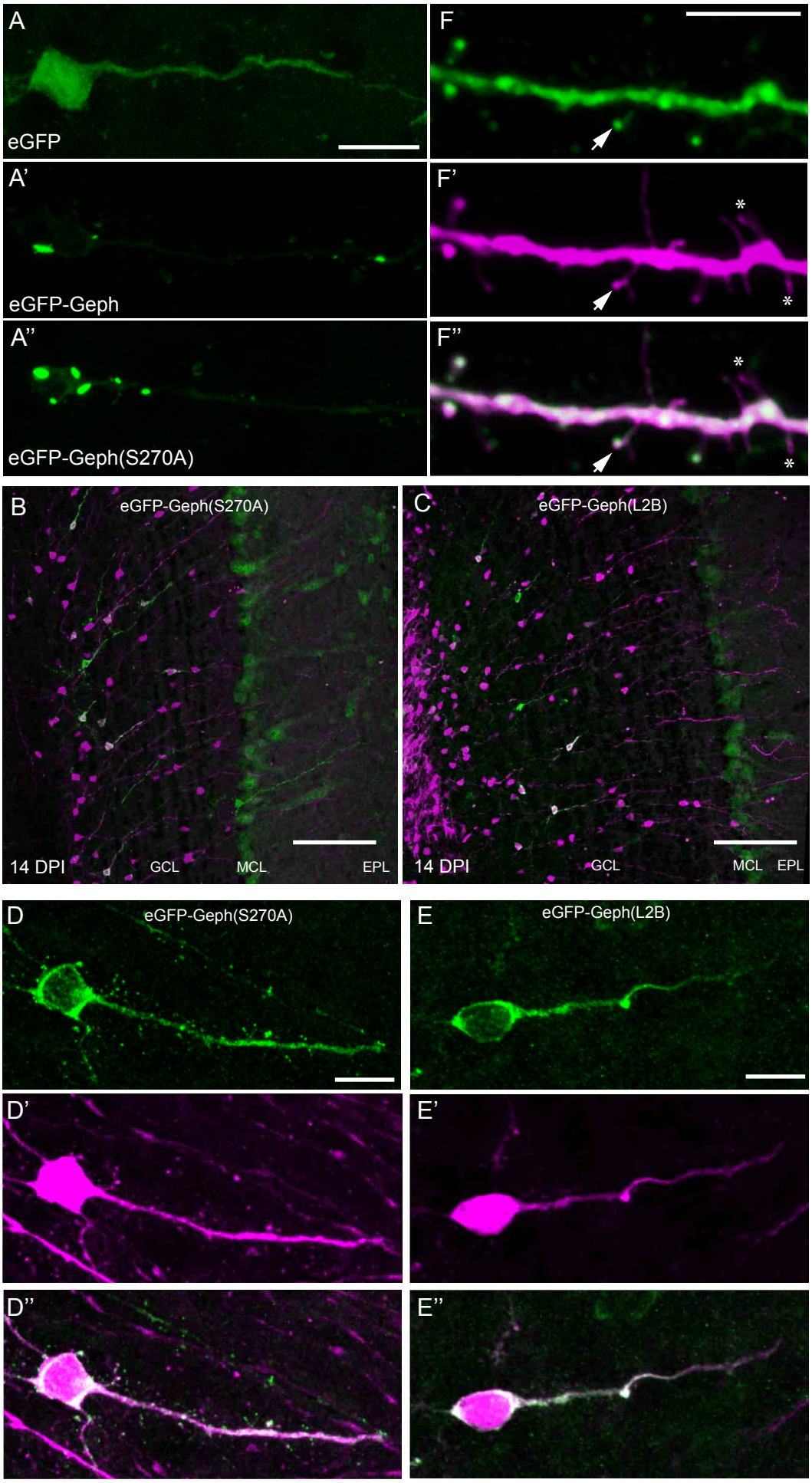
A
eGFP
A'
eGFP-Geph
A''
eGFP-Geph(S270A)
F
F'
F''
B
eGFP-Geph(S270A)
14 DPI
GCL
MCL
EPL
C
eGFP-Geph(L2B)
14 DPI
GCL
MCL
EPL
D
eGFP-Geph(S270A)
D'
D''
E
eGFP-Geph(L2B)
E'
E''

Figure 1

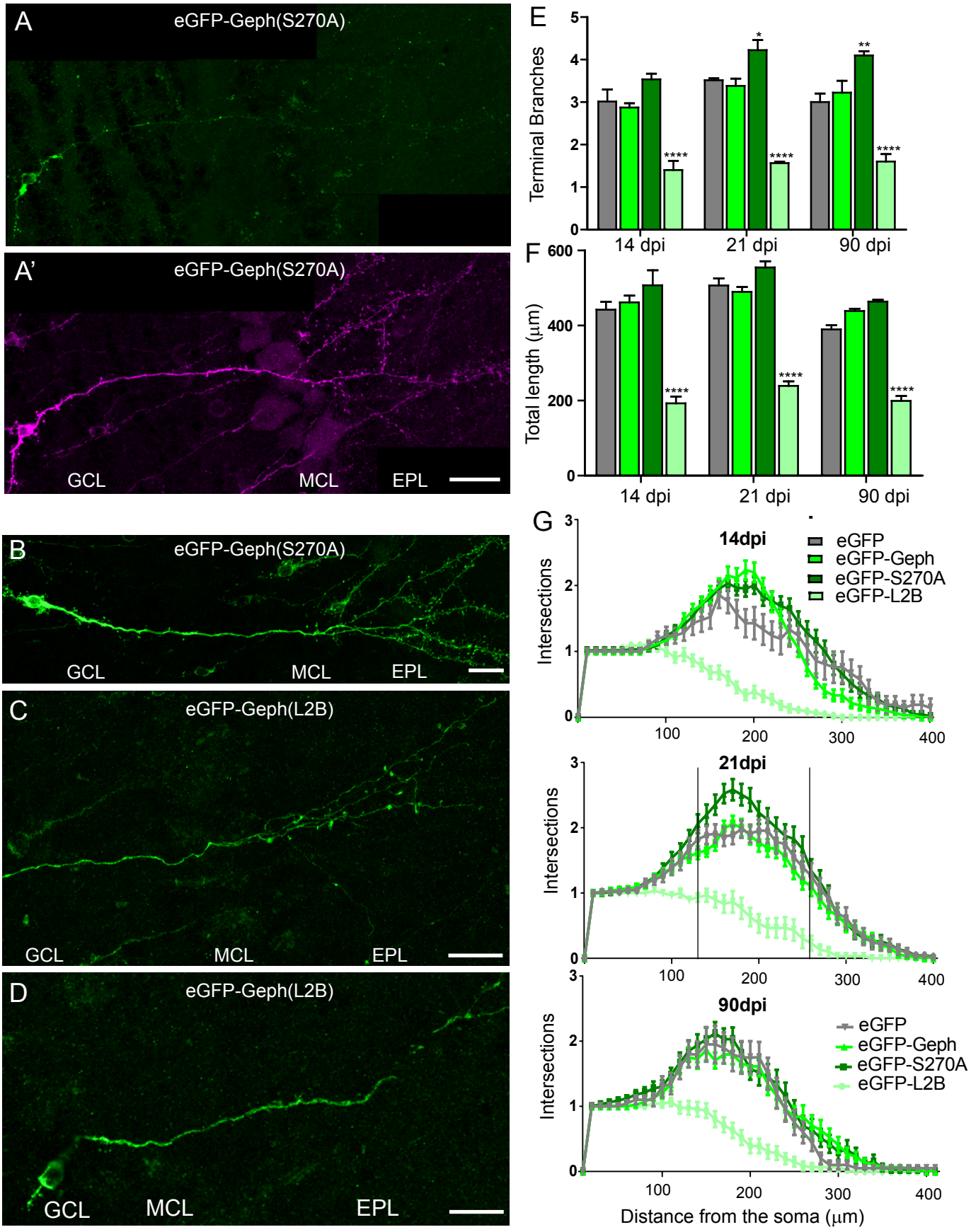
A
eGFP-Geph(S270A)
A'
eGFP-Geph(S270A)
GCL
MCL
EPL
B
eGFP-Geph(S270A)
GCL
MCL
EPL
C
eGFP-Geph(L2B)
GCL
MCL
EPL
D
eGFP-Geph(L2B)
GCL
MCL
EPL
E
Terminal Branches
14 dpi
21 dpi
90 dpi
F
Total length (μm)
14 dpi
21 dpi
90 dpi
G
14dpi
21dpi
90dpi
Intersections
eGFP
eGFP-Geph
eGFP-S270A
eGFP-L2B
Distance from the soma (μm)

Figure 2

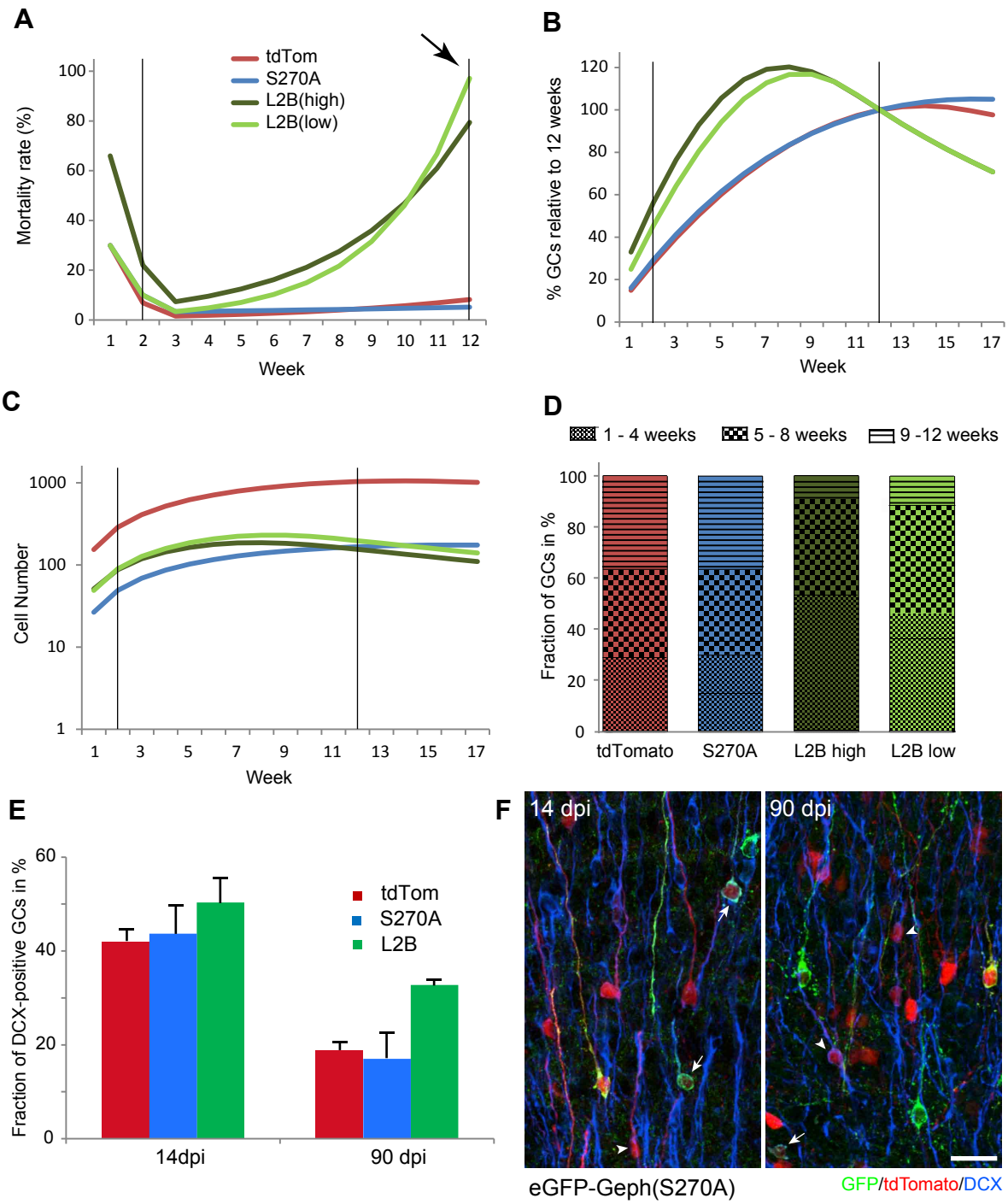
A
Mortality rate (%)
tdTom
S270A
L2B(high)
L2B(low)
Week
B
% GCs relative to 12 weeks
Week
C
Cell Number
Week
D
1 - 4 weeks
5 - 8 weeks
9 -12 weeks
Fraction of GCs in %
tdTomato
S270A
L2B high
L2B low
E
Fraction of DCX-positive GCs in %
tdTom
S270A
L2B
14dpi
90 dpi
F
14 dpi
90 dpi
eGFP-Geph(S270A)
GFP/tdTomato/DCX

Figure 3

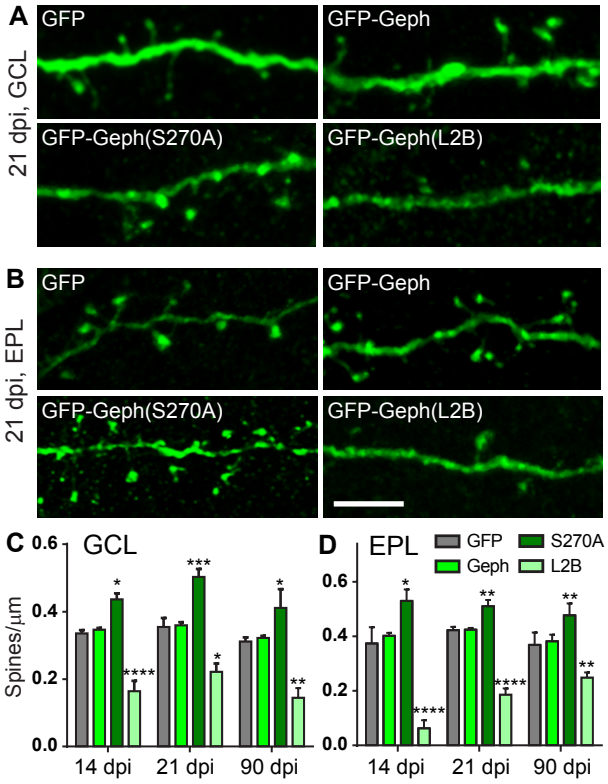
A
GFP
GFP-Geph
21 dpi, GCL
GFP-Geph(S270A)
GFP-Geph(L2B)
B
GFP
GFP-Geph
21 dpi, EPL
GFP-Geph(S270A)
GFP-Geph(L2B)
C
GCL
Spines/µm
0.6
0.4
0.2
0.0
14 dpi
21 dpi
90 dpi
D
EPL
GFP
S270A
Geph
L2B

Figure 4

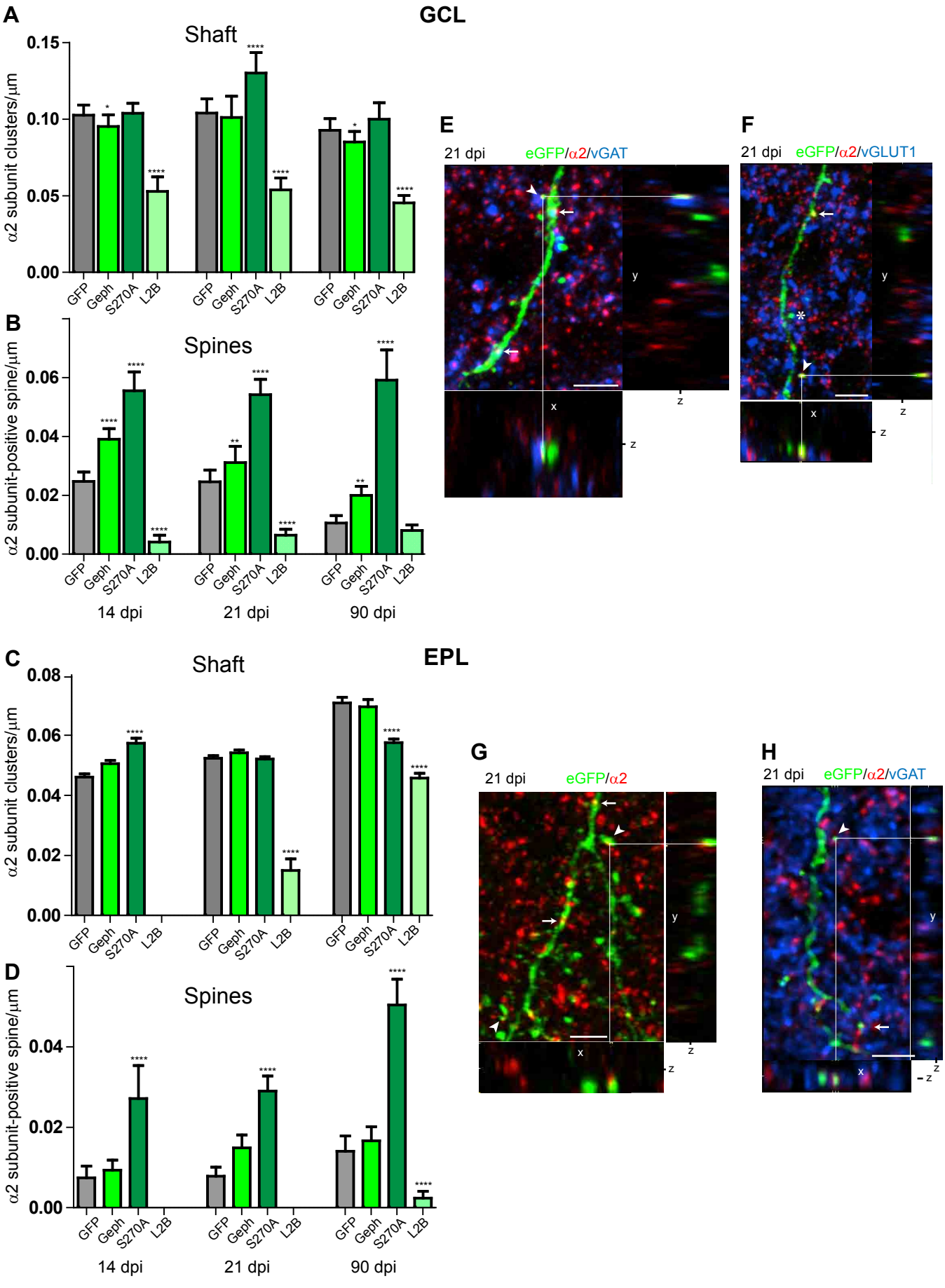
A
GCL
Shaft
α2 subunit clusters/µm
0.15
0.10
0.05
0.00
GFP
Geph
S270A
L2B
B
Spines
α2 subunit-positive spine/µm
0.06
0.04
0.02
0.00
14 dpi
21 dpi
90 dpi
E
21 dpi
eGFP/α2/vGAT
F
21 dpi
eGFP/α2/vGLUT1
C
EPL
Shaft
0.08
D
Spines
0.04
G
21 dpi
eGFP/α2
H
21 dpi
eGFP/α2/vGAT

Figure 5

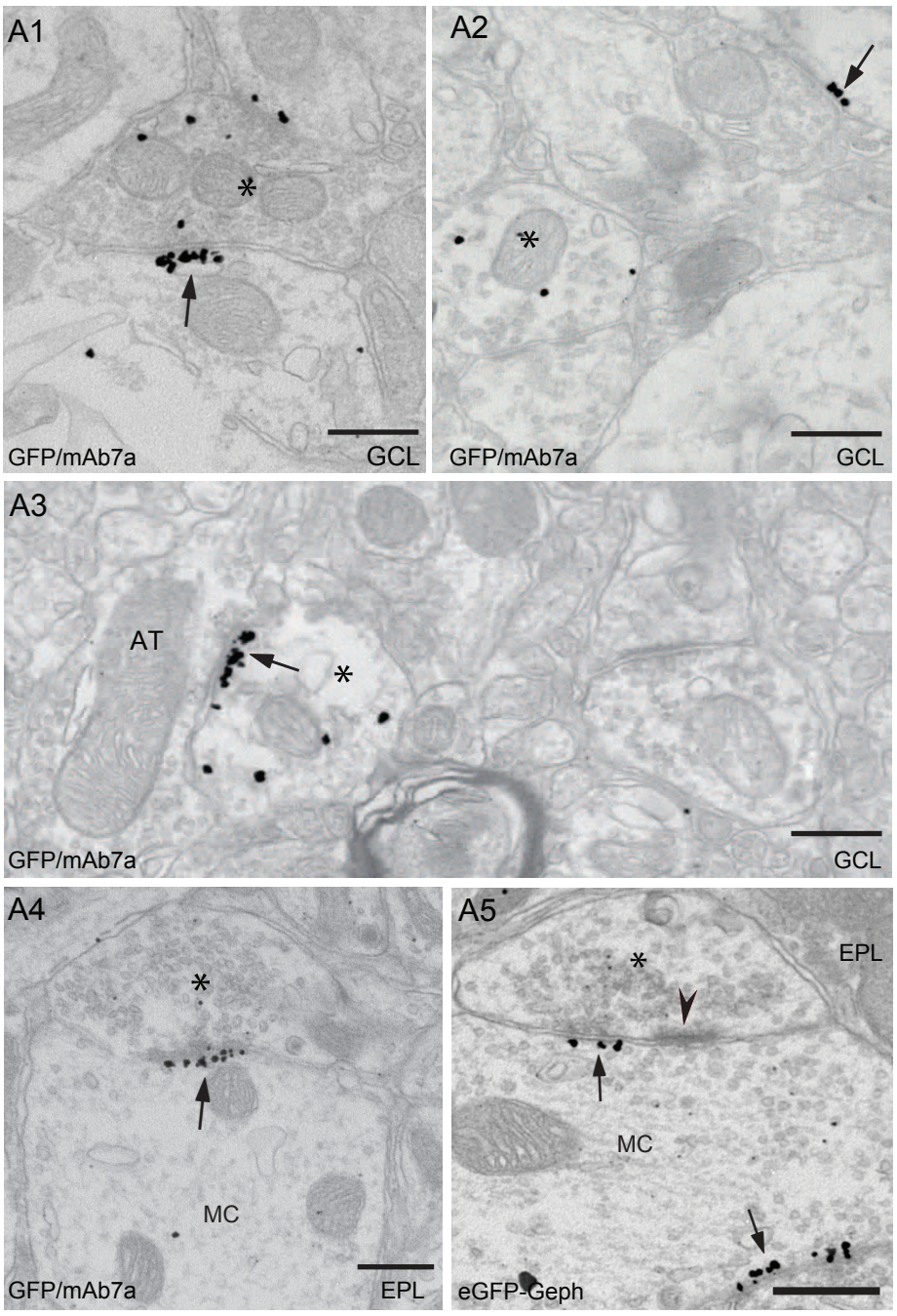
A1
GFP/mAb7a
GCL
A2
GFP/mAb7a
GCL
A3
AT
GFP/mAb7a
GCL
A4
MC
GFP/mAb7a
EPL
A5
EPL
MC
eGFP-Geph

Figure 6A

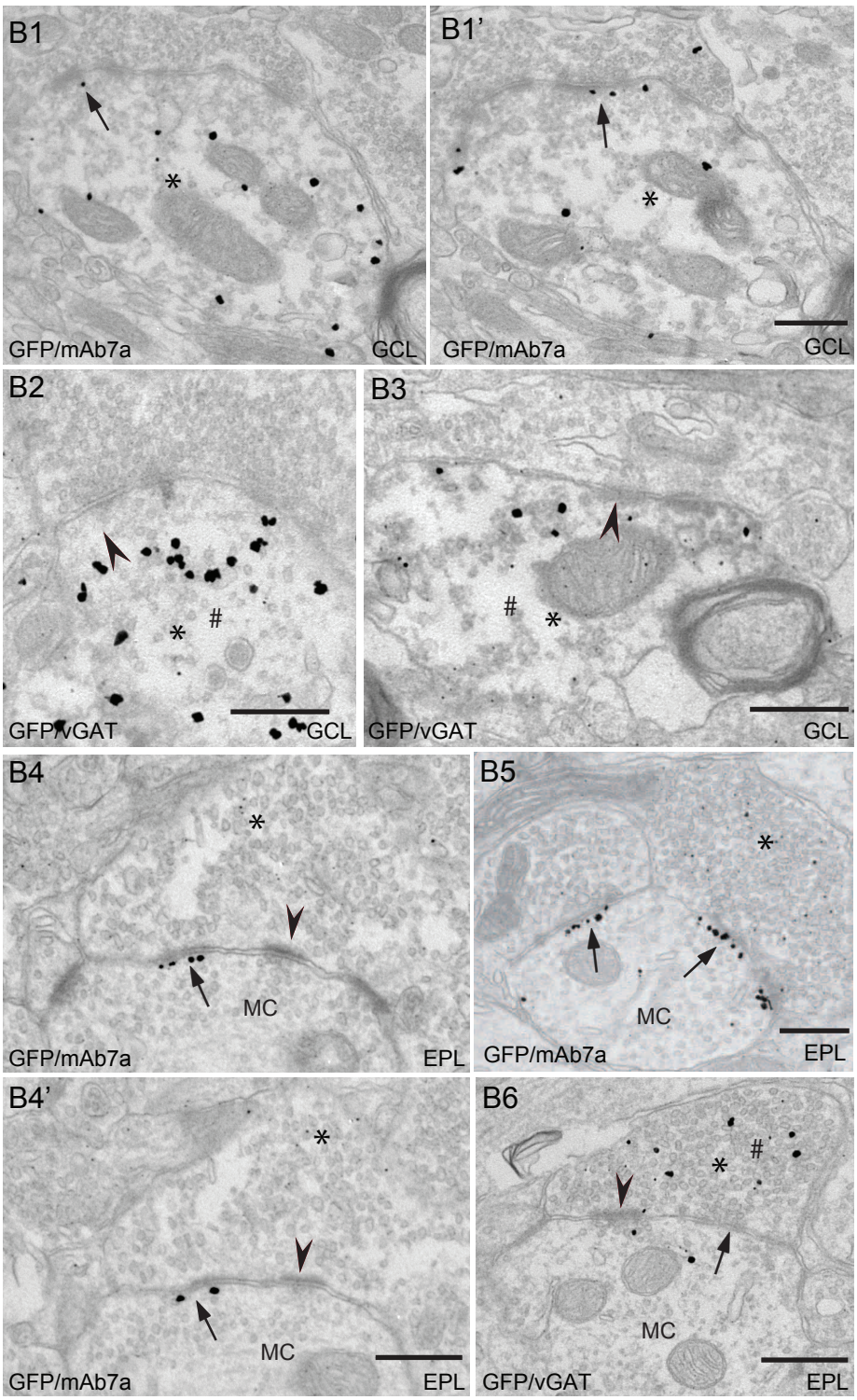
B1
GFP/mAb7a
GCL
B1'
GFP/mAb7a
GCL
B2
GFP/vGAT
GCL
B3
GFP/vGAT
GCL
B4
MC
GFP/mAb7a
EPL
B5
MC
GFP/mAb7a
EPL
B4'
MC
GFP/mAb7a
EPL
B6
MC
GFP/vGAT
EPL

Figure 6B

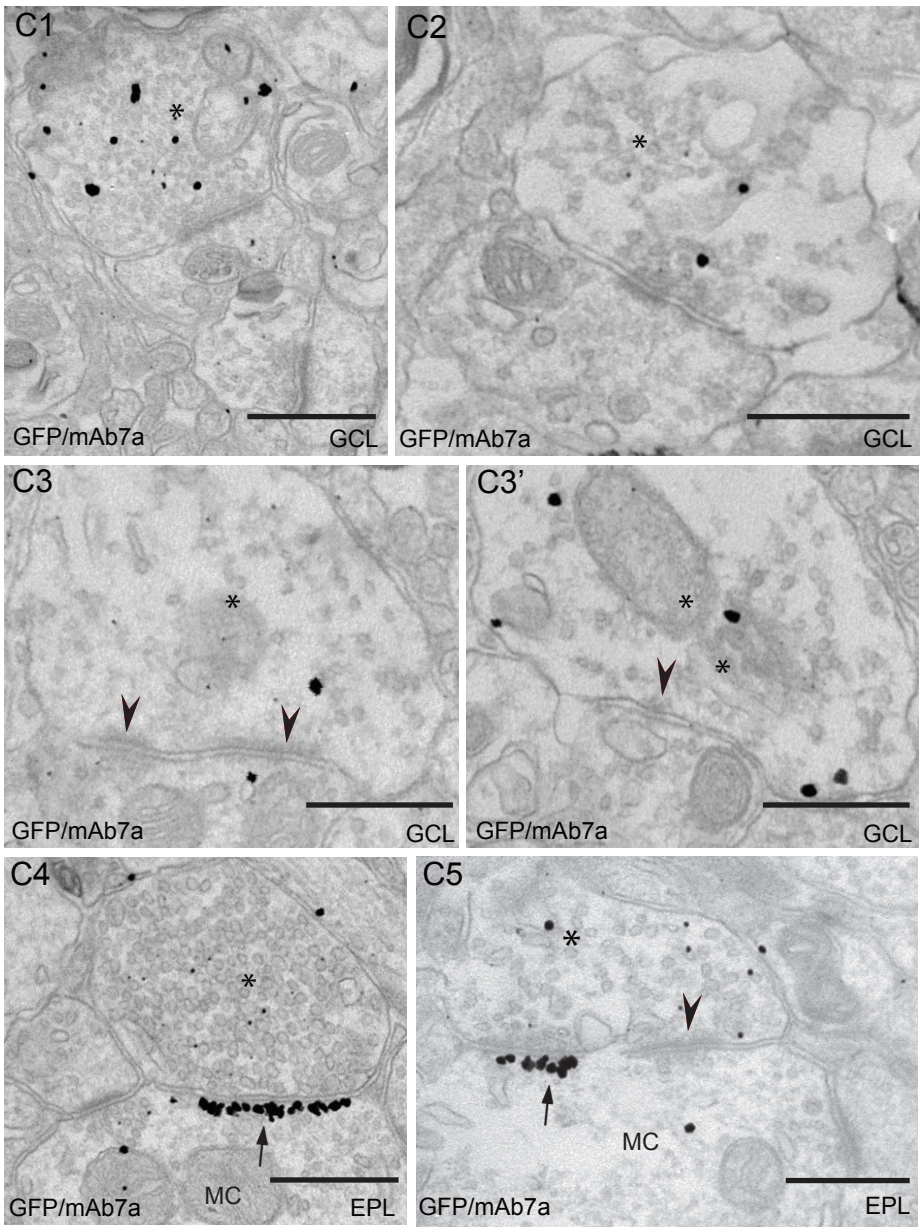
C1
GFP/mAb7a
GCL
C2
GFP/mAb7a
GCL
C3
GFP/mAb7a
GCL
C3'
GFP/mAb7a
GCL
C4
MC
GFP/mAb7a
EPL
C5
MC
GFP/mAb7a
EPL

Figure 6C

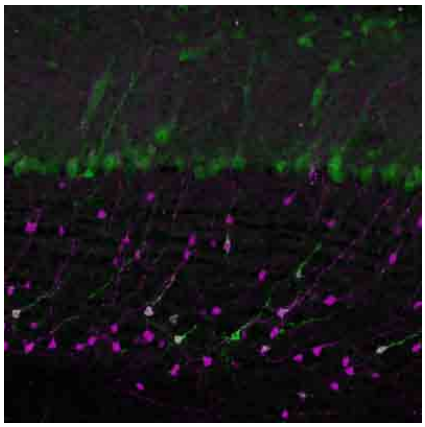

Graphical abstract
Deprez et al., JCN